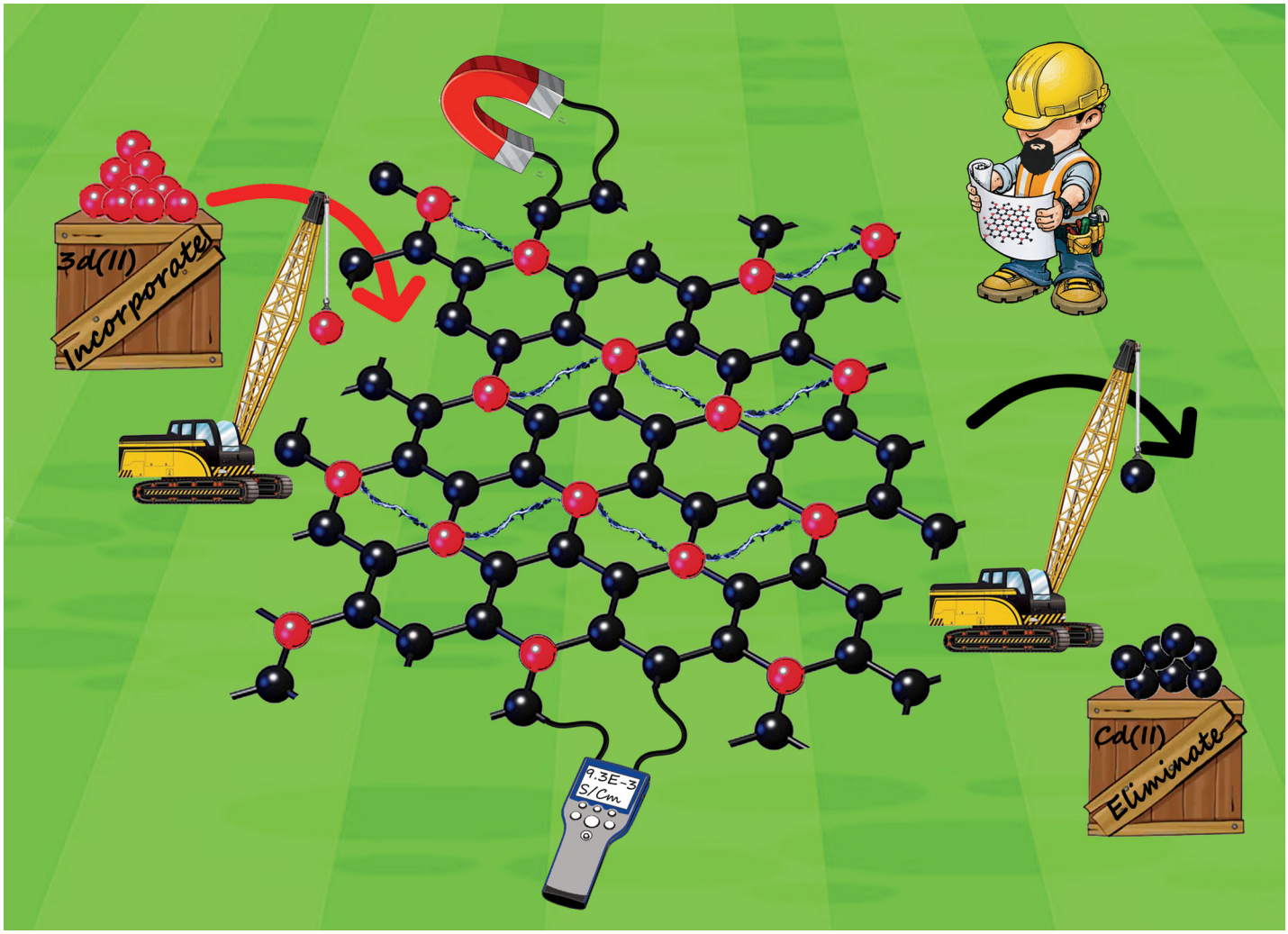

Showcasing the collaborative research of the Pablo Fuentealba group from Departamento de Química Inorgánica y Analítica, Facultad de Ciencias Químicas y Farmacéuticas, Universidad de Chile, and LIA/3M Project of Université de Rennes 1, CEPID Project of Universidade de Sao Paulo, and Instituto de Física of Universidade Federal de Goiás.

Physical properties of new ordered bimetallic phases $M_{0.25}Cd_{0.75}PS_3$ ($M = Zn^{II}$, Ni^{II}, Co^{II}, Mn^{II})

Layered bimetallic phases of the thiophosphate family are synthesized by the cationic exchange reaction. An ordered distribution of the inserted 3d ions is assessed, which is related to the observed physical properties. Physical properties such as magnetism, conductivity and solid state absorption are investigated.

As featured in:

See P. Fuentealba *et al.*, *Phys. Chem. Chem. Phys.*, 2020, **22**, 8315.

ROYAL SOCIETY OF CHEMISTRY

rsc.li/pccp

Registered charity number: 207890

PCCP

PAPER

View Article Online
View Journal | View Issue

Cite this: *Phys. Chem. Chem. Phys.*, 2020, **22**, 8315

Physical properties of new ordered bimetallic phases $M_{0.25}Cd_{0.75}PS_3$ (M = Zn^{II}, Ni^{II}, Co^{II}, Mn^{II})†‡

P. Fuentealba, *[ab] C. Olea,[a] H. Aguilar-Bolados,[a] N. Audebrand,[c] R. C. de Santana,[d] C. Doerenkamp,[e] H. Eckert,[e] C. J. Magon[e] and E. Spodine[ab]

Received 4th February 2020,
Accepted 2nd March 2020

DOI: 10.1039/d0cp00631a

rsc.li/pccp

Four bimetallic phases of the thiophosphate family have been synthesized by the cationic exchange reaction using a freshly prepared $K_{0.5}Cd_{0.75}PS_3$ precursor phase and methanolic solutions of nitrates of the divalent cations Zn^{II}, Ni^{II}, Co^{II}, and Mn^{II}. All the materials were characterized by FTIR, PXRD, SEM-EDXS and (in the case of the diamagnetic compounds) by solid state NMR. For the $K_{0.5}Cd_{0.75}PS_3$ precursor, the X-ray powder diffraction data suggest a modification of the structure, while solid state NMR results confirm that this phase possesses an ordered arrangement of Cd vacancies. The cationic exchange reaction achieves a complete removal of potassium ions (no potassium detected by SEM-EDXS) and re-occupation of the vacancies by divalent cations. Therefore, the obtained compounds have an average composition of $M_{0.25}Cd_{0.75}PS_3$ (M = Zn^{II}, Ni^{II}, Co^{II}, Mn^{II}) and possess an ordered distribution of the substituent cations. Even with the paramagnetic substitution level of 25%, antiferromagnetic behaviour is present in the phases with Mn^{II}, Co^{II} and Ni^{II}, as evidenced by dc susceptibility and in the case of the Mn^{II} substituted phase by EPR. The cooperative magnetic interactions confirm the conclusion that the paramagnetic ions adopt an ordered arrangement. The analysis by broad band impedance spectroscopy allows to attribute the conductivity in these materials to charge movements in the layers due to the difference in electronegativity of the metal ions. $Zn_{0.25}Cd_{0.75}PS_3$ is the phase that shows the highest conductivity values. Finally, the band gap energies of the bimetallic phases tend to be lower than those of the single-metal phases, probably due to an overlap of the band structures.

Introduction

Transition metal thiophosphate phases are a well-known family of layered compounds whose properties are the focus of interest for many researchers. Even though these compounds were first reported in 1965,[1] pristine phases are still under analysis.[2–4] The structure of these materials is well known: the ethane like $P_2S_6^{4-}$ ligands provide an octahedral environment of sulfur atoms to the transition metal ions, which are in a hexagonal arrangement within the layers.[5] In one of the last reviews reported on this family of lamellar phases[6] the importance of these materials is highlighted, together with the description of their properties, such as catalytic activity, charge transport, and antiferromagnetism. Furthermore, some of these materials have been analyzed as potential systems for Li batteries[7] or for H_2 storage.[4,8] They have also served to create materials with other important layered compounds such as graphene.[9]

Due to their interesting intercalation chemistry and potential applications, different methods have been developed to obtain new phases, and many studies have been devoted to the modification of their physical properties, by introducing in the interlayer space different chemical species, such as cations,[10] complexes,[11–15] radicals,[16] and polymers,[17,18] among others. An important aspect of these intercalation reactions is that when these charged species are introduced in the pristine phases, an ordered network of vacancies is created, which are relevant for the physical properties of the final composites.[19,20]

Another route to modify the properties of the thiophosphate phases is by the substitution of some of the elements that form the layers. It is possible to change the chalcogenide, obtaining phases with sulfur and selenium, and it is possible to replace the transition metal ion. Many combinations of transition metal ions have been

[a] *Facultad de Ciencias Químicas y Farmacéuticas, Universidad de Chile, Santiago, Chile. E-mail: pfuentealbacastro@ciq.uchile.cl*
[b] *Centro para el Desarrollo de Nanociencias y Nanotecnología, CEDENNA, Santiago, Chile*
[c] *Univ Rennes, CNRS, ISCR (Institut des Sciences Chimiques de Rennes) – UMR 6226, F-35000 Rennes, France*
[d] *Instituto de Física, Universidade Federal de Goiás, Goiânia, Brazil*
[e] *Instituto de Física de São Carlos, Universidade de São Paulo, São Carlos, Brazil*

† This manuscript is dedicated to Jean-René Hamon on the occasion of his 65th birthday.

‡ Electronic supplementary information (ESI) available: FTIR spectra, PXRD diffractograms and simulated patterns, $M(H)$ curves, EPR spectra and equations used for magnetic fittings. See DOI: 10.1039/d0cp00631a

used, $3d^{II}$–$3d^{II}$,[21,22] $3d^{II}$–$4d^{II}$,[23,24] or combination with 3+ cations, such as aluminium, gallium, indium have been reported.[25] Lanthanide(III) ions have also been involved in some heteronuclear phases, combined with sodium or potassium ions.[26,27] Nevertheless, most of these phases have been obtained by the ceramic method, and in the case of heterometallic phases with 3d–3d and 3d–4d cations, a random distribution of the transition ions is achieved.[28]

Due to the great relevance of these materials, based on their potential applications,[6] it is important to have a more controlled synthetic procedure to avoid this random distribution in order to obtain an ordered material. In our group, we have been working with a two-step methodology, using the intercalation reaction, to achieve ordered bimetallic phases.[29,30] In the present work the characterization of four new ordered bimetallic phases, derived from $CdPS_3$, together with their magnetic, conducting and optical properties are reported. The analysis of their properties indicates that the ordered distribution of the inserted ions is related to the observed experimental properties.

Experimental

Synthesis

Pure elements (Cd, S, P, 99.9%) were dried under vacuum before doing the solid state reaction. Cadmium, sulfur, phosphorus, iodine, potassium chloride, nitrate salts and methanol were used as received from commercial sources.

The synthesis of $CdPS_3$ was done by the ceramic method using iodine as vapor transport agent to improve the crystallinity of the obtained solid. Stoichiometric 1 : 1 : 3 mixtures of the pure elements Cd, P and S, calculated to obtain 1 g of compound, were ground with 10–15 mg of iodine, and sealed in quartz tubes in an argon atmosphere. The reaction was done at 750° for two weeks. The obtained solid was washed with carbon disulphide to remove remaining iodine, and finally, the product was washed with methanol and dried under vacuum. EDXS calculated/experimental for $CdPS_3$: Cd, 46.92/44.6(3); P, 12.93/13.8(2); S, 40.1/41.5(2).

The potassium precursor was obtained by stirring 200 mg of the pristine $CdPS_3$ phase in 20 mL of a 2 M KCl solution, with 10 mL 0.1 M of EDTA, prepared in a potassium carbonate buffer solution (K_2CO_3/$HKCO_3$) at pH 9 for 24 hours at room temperature. EDXS calculated/experimental for $K_{0.5}Cd_{0.75}PS_3$: K, 8.46/9.33(1); Cd, 36.49/35.2(2); P, 13.41/13.6(1); S, 41.64/41.8(4).

The bimetallic phases were obtained by stirring the freshly prepared potassium precursor for 24 hours in a methanol solution of the corresponding divalent ion. The quantity of nitrate salt ($M(NO_3)_2{\cdot}xH_2O$, M = Mn^{II}, Co^{II}, Ni^{II} or Zn^{II}) to be used was calculated based on the potassium present in the precursor, using a twofold excess (Table 1).

Table 1 Elemental analysis obtained by EDX spectroscopy

	Ni^{II}	Co^{II}	Mn^{II}	Zn^{II}
Cd	37.28 (36.8(3))	37.27 (37.6(6))	37.44 (37.1(2))	37.01 (36.6(2))
P	13.70 (13.5(5))	13.69 (13.8(3))	13.75 (13.9(7))	13.60 (13.1(7))
S	42.54 (42.1(4))	42.53 (42.9(5))	42.71 (43.0(3))	42.22 (42.1(3))
M	6.49 (6.4(3))	6.51 (6.6(5))	6.10 (6.2(4))	7.17 (7.0(4))

Physical characterizations

Equipments

SEM-EDXS analyses were performed on a JEOL scanning microscope (JSM-5410), with an Oxford Lin Isis energy dispersive X-ray detector.

^{113}Cd Solid state NMR spectra were recorded at 5.7 T (resonance frequency 53.78 MHz) with an Agilent DD2 spectrometer, using a 4 mm probe operated at a rotation frequency of 5000 Hz. Data were acquired with 90° pulses of 2.5 μs length. Chemical shifts are referenced to 1 M $Cd(NO_3)_2$ solutions, using crystalline $CdPS_3$ as a secondary standard at 480 ppm. ^{31}P solid state NMR spectra were measured on a Bruker Avance Neo 600 MHz spectrometer (resonance frequency 243.03 MHz), using a 3.2 mm probe operated at a spinning frequency of 10 000 Hz. Data were acquired with 90° pulses of 5 μs length and relaxation delay of 2000 s. Chemical shifts are reported relative to 85% H_3PO_4 using solid BPO_4 (−29.3 ppm) as a secondary standard.

Powder X-ray diffraction patterns were collected from 5° to 100° 2θ, on a Bruker D8 Advance diffractometer, equipped with a LynxEye detector, and operation with monochromatic Cu $K\alpha_1$ radiation selected with a Ge monochromator. The obtained diffractograms were refined with Le Bail algorithm with the FullProf software in the WinPLOTR interface.[31,32]

The dc magnetic susceptibilities were measured under an external applied field of 100 Oe, from 2 K to 300 K, using a Quantum Design Dynacool Physical Properties Measurement System (PPMS), equipped with a Vibrating Sample Magnetometer (VSM).

The EPR spectra were recorded on a Bruker Elexsys E-580 spectrometer, equipped with a standard Bruker rectangular cavity. A continuous flow liquid helium cryostat, model ESR-900, and a PID controller model ITC503, both from Oxford Instruments, were used to control the temperature.

Dielectric properties were measured on a disk of pressed powder of 10 mm diameter and *ca.* 200 μm of thickness at 23 °C, over the frequency range window of 10^{-1} to 10^{7} Hz in a broadband dielectric spectrometer from Novocontrol Technologies GmbH (model BDS-40). Each sample was held between two parallel gold-plated electrodes and its thickness measured using a micrometer gauge. The amplitude of the applied AC electric signal was 1 V. The complex conductivity (σ^*) and the electric modulus (M^*) are given directly by the analyser.

Diffuse reflectance spectra were measured on a PerkinElmer Lambda WB1050 spectrophotometer, equipped with a Praying Mantis diffuse reflection accessory.

Results and discussion

General characterization

The pristine $CdPS_3$ phase and the product after the first cationic exchange reaction ($K_{0.5}Cd_{0.75}PS_3$), were characterized by SEM-EDXS and powder X-ray diffraction in order to certify the quality of the initial materials for the preparation of the bimetallic phases. The obtained stoichiometries are $CdPS_3$

Table 2 Obtained unit cell for the layered phases

	$CdPS_3$	$Mn_{0.25}Cd_{0.75}PS_3$	$Co_{0.25}Cd_{0.75}PS_3$
S.G.	*C*2/*m*	*P*2/*m*	*P*2/*m*
a (Å)	6.2192(1)	6.1842(2)	6.1445(8)
b (Å)	10.7513(4)	10.68157(7)	10.687(1)
c (Å)	6.8788(1)	6.87844(2)	6.8821(6)
β (°)	107.724(2)	107.839(3)	107.97(1)

	$Ni_{0.25}Cd_{0.75}PS_3$	$Zn_{0.25}Cd_{0.75}PS_3$
S.G.	*P*2/*m*	*P*2/*m*
a (Å)	6.0811(8)	6.1998(4)
b (Å)	10.731(2)	10.7309(6)
c (Å)	6.8816(8)	6.8810(5)
β (°)	108.08(1)	107.859(5)

and $K_{0.5}Cd_{0.75}PS_3$. FTIR spectroscopy provides evidence of the formation of the vacancies within the layers; the FTIR spectrum of the pristine $CdPS_3$ phase shows two bands at 570 and 450 cm^{-1} due to the vibration of the PS_3 groups and the P–P bond respectively. However, the infrared spectra of the $K_{0.5}Cd_{0.75}PS_3$ phase shows a splitting of the PS_3 vibration bands (Fig. S1, ESI‡) after the insertion of the K^+ cations, due to the modification of the local environment of the PS_3 ligand after the partial removal of the Cd^{II} cations from the layers. The diffractogram of the pristine phase was analyzed by the Le Bail method, in order to corroborate the purity of the obtained material, found to be the only crystalline phase identified. The obtained unit cell parameters (Table 2) are similar to the reported ones.[6,33] The diffractogram of the potassium precursor evidences a structural modification of the pristine phase (Fig. S2, ESI‡). Due to the rather medium quality of the data, only few diffraction lines are observed. Nevertheless, based on these data an indexing has been attempted with the program Dicvol14[34] and a possible unit-cell in monoclinic system (in space groups *P*2, *Pm* or *P*2/*m*) would be 6.6006(5) Å, 6.5228(3) Å, 9.2282(2) Å, 94.150(5)°, suggesting an increase in the layer-to-layer distance from 6.5 to 9.4 Å (distance calculated using the 001 diffraction line). It would then indicate the presence of the monovalent cations in the interlamellar space. Therefore, it is an indication of a modification in the structure by the intercalation of potassium ions and as a consequence the creation of some vacancies on metal sites of the layers. Similar experimental observations have been reported with organic intercalates.[20]

All lamellar phases obtained from $K_{0.5}Cd_{0.75}PS_3$ were also characterized by SEM-EDXS in order to estimate the composition. No remaining potassium was observed by EDXS, proving that a complete exchange was achieved.

The obtained phases have an average stoichiometry of $M'_{0.25}Cd_{0.75}PS_3$, where M′ is Zn^{II}, Co^{II}, Ni^{II} and Mn^{II}. Furthermore, FTIR spectra of the bimetallic phases show a single vibration band for the $-PS_3$ group (Fig. S1, ESI‡), making evident that the existing vacancies in $K_{0.5}Cd_{0.75}PS_3$ have been filled by the 3d ions. The insertion of the 3d ions is facilitated by their smaller ionic radii compared to cadmium(II) cations (Table S1, ESI‡). This phenomenon was also observed in a precious study of the $K_{0.4}Mn_{0.8}PS_3$ phase, whose vacancies can be filled by Ni^{II}, Co^{II}, Cu^{II} and Zn^{II} ions.[29,30]

Powder X-ray diffractograms of the bimetallic phases were recorded in order to analyze the crystalline structure of the obtained bimetallic phases. All obtained phases show interlamellar distances of 6.5 Å, similar to that of the pristine $CdPS_3$ phase. The observed maxima of the 00*l* planes for the bimetallic phases are broader than those of the pristine phase, indicating a loss of the crystallinity after the intercalation and exchange reactions. Diffractograms of the bimetallic phases have been indexed and fitted using a monoclinic *P*2/*m* unit cell, indicating a modification of the structure of $CdPS_3$ phase. The obtained unit cell parameters are closely related to those of the pristine $CdPS_3$ phase.

Solid state NMR spectroscopy

All diamagnetic compounds have been characterized by solid state NMR spectroscopy, in order to confirm the successful syntheses. Furthermore, ^{31}P (Fig. 1) and ^{113}Cd NMR spectra (Fig. 2) provide the needed information about the local environment of the ligand and the metallic centre.

The ^{31}P spectrum of $CdPS_3$ consists of a main peak at 103.7 ppm (and a weak peak around 101 ppm attributed to an impurity) demonstrating a singular and uniform phosphorus environment. After the first ion exchange, the spectra show several components: a doublet at 102.4 ppm ($^1J(^{31}P–^{31}P)$ = 146 Hz), and three singlets at 99.4, 97.7 and 96.6 ppm. As previously reported, and fully discussed by Schmedt auf der Günne and coworkers,[35] the freshly synthesized potassium precursor ($K_{0.5}Cd_{0.75}PS_3$) has vacancies within the layers, while the potassium ions occupy the interlayer space. As previously discussed, the signal at 102.4 and the *J*-doublet at 97.7/96.6 ppm arise from $P_2S_6^{4-}$ groups that are situated near two and one vacancies, respectively. From their 1 : 1 intensity ratio we can conclude that the vacancy distribution is perfectly ordered, and no $P_2S_6^{4-}$ groups near zero and three vacancies can be found. The additional signal at 99.4 ppm arises from $P_2S_6^{4-}$ groups near potassium ions that are situated within the layers (see below). Even though the present potassium compound was obtained by a different synthetic procedure in comparison with ref. 35, the spectra of

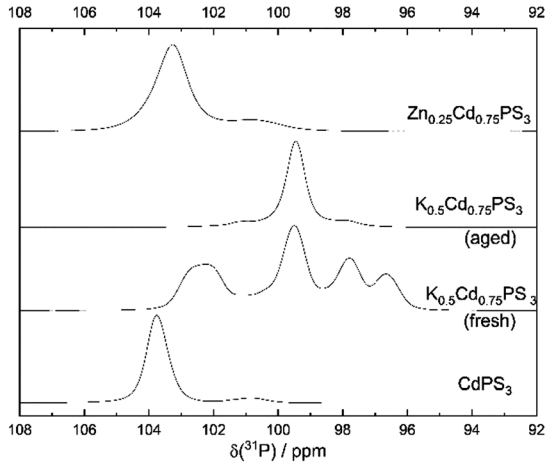

Fig. 1 ^{31}P NMR spectra of the studied phases.

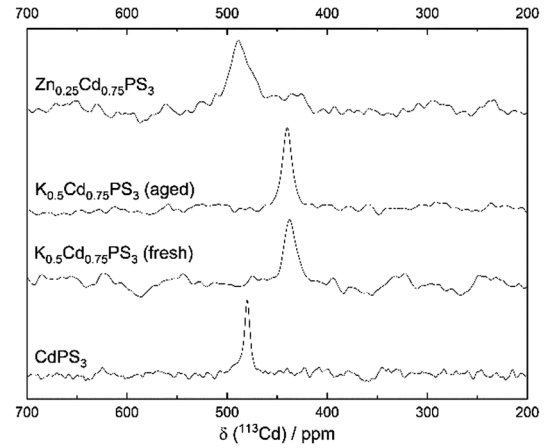

Fig. 2 ^{113}Cd NMR spectra of the studied phases.

both materials look almost identical. The ratio of vacancies to Cd^{II} sites is 1:4, as established by the stoichiometry, which together with the NMR results, indicates that the vacancy distributions are the same. As was already observed, these vacancies vanish with time, leading to the emergence of a dominant central peak at 99.5 ppm, flanked by two weaker signals at 101 and 98 ppm. This can be explained by the migration of potassium ions into these vacancies and highlights the importance of using a freshly synthesized potassium precursor for the subsequent ion exchange reactions.

When the freshly prepared potassium intercalation compound is treated with a solution of diamagnetic ions, the vacancies are filled by the latter and the potassium ions are removed from the interlayer space. For the Zn^{II} exchanged sample, the dominant ^{31}P resonance at 103.3 ppm reflects this situation, while some weaker signals attributed to amorphous impurities at 90 and 125 ppm are observed as well. In the case of the Mn^{II}, Co^{II}, and Ni^{II}-exchanged samples, the NMR signals are suppressed by the strong magnetic interactions.

The ^{113}Cd NMR spectrum of the pristine phase, shown in Fig. 2, is characterized by a single resonance at 480 ppm. By introducing potassium ions, we observe a significant displacement to lower values towards 439 ppm, but no additional resonances appeared. Again, this result agrees very well with previous work on freshly prepared $K_{0.5}Cd_{0.75}PS_3$. Contrary to the ^{31}P spectra of the potassium precursor, we do not observe any change in the signal with time for the ^{113}Cd resonance. This is easily explained by the fact that the Cd^{II} environment remain unaffected by the K^+ migration process. After the subsequent ion exchange with Zn^{II}, the main peak is shifted back to a value of 490 ppm, which is similar to the one of the pristine phase, and thus complements and confirms the conclusions from the ^{31}P spectra. The data are consistent with the migration of Zn^{II} ions into the created vacancies of $K_{0.5}Cd_{0.75}PS_3$, which leads to a uniform environment around the $P_2S_6^{4-}$ ligands and the Cd^{II} ions, similar to the situation in the original $CdPS_3$ phase.

Magnetic properties

Magnetic susceptibility

The magnetic analysis of the bimetallic phases with Ni^{II}, Co^{II} and Mn^{II} was done using dc magnetic measurements and EPR spectroscopy. $\chi_M(T)$ and χ_M^{-1} (T) for (a) $Mn_{0.25}Cd_{0.75}PS_3$, (b) $Ni_{0.25}Cd_{0.75}PS_3$ and (c) $Co_{0.25}Cd_{0.75}PS_3$ plots are shown in Fig. 3.

The $\chi_M(T)$ curves can be reasonably fitted using a modified Curie Weiss equation[36,37] (see Supplementary Data Section for equations, ESI‡). The Weiss temperature values θ obtained for all the compounds, calculated using the high temperature range of $\chi_M^{-1}(T)$ curves, together with the obtained parameters from the fitting are summarized in Table 3. The negative values are indicative of bulk antiferromagnetic interactions between the M^{II} ions, and were found to be lower than those measured for the respective pristine phases. In the case of $Mn_{0.25}Cd_{0.75}PS_3$, the obtained θ value agrees very well with those obtained by Zhang *et al.*[39] for $Mn_xCd_{1-x}PS_3$, −270.5, −199.3, −114.2 and −39.7 K for x = 1, 0.82, 0.52 and 0.2, respectively, following an almost linear dependence, as shown in Fig. 4. The Curie constants, obtained from the slope of the $1/\chi_M$ *vs.* T data in the high-temperature region allow us to calculate the effective magnetic

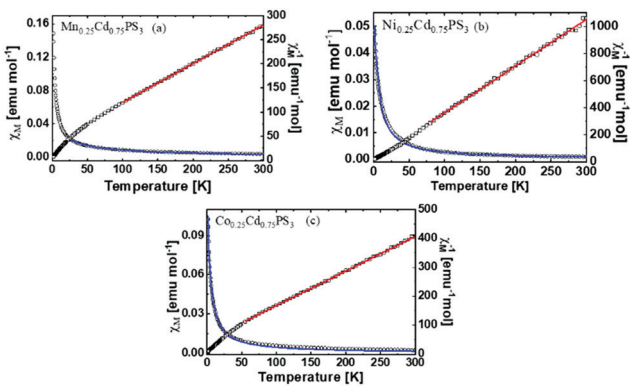

Fig. 3 Magnetic susceptibility plots $\chi_M(T)$ (blue curves) and χ_M^{-1} (T) (red curves) for (a) $Mn_{0.25}Cd_{0.75}PS_3$, (b) $Ni_{0.25}Cd_{0.75}PS_3$ and (c) $Co_{0.25}Cd_{0.75}PS_3$. Solid lines correspond to the fit of the experimental data as explained in the text.

Table 3 μ_{eff}, μ_{SO} (spin only value), θ and J values for $M_{0.25}Cd_{0.75}PS_3$ phases (M^{II} = Ni, Co, Mn)

Sample	μ_{eff} (μ_B)	μ_{SO} (μ_B)	θ (K)	$\lvert J/k_B \rvert$ (K)
$Mn_{0.25}Cd_{0.75}PS_3$	3.16(4)	2.96	−50.6(7)	8.0(8)[a]
$Ni_{0.25}Cd_{0.75}PS_3$	1.52(5)	1.414	−5(1)	2.17(3)[a]
$Co_{0.25}Cd_{0.75}PS_3$	2.58(2)	1.936	−39(1)	1.52(8)[a]
$MnPS_3$[38]	5.72(3)	5.92	−250(1)	8.3(2)[a]
$Mn_{0.82}Cd_{0.18}PS_3$[39]	n.a.	5.36	−199.3	n.a.
$Mn_{0.52}Cd_{0.48}PS_3$[39]	n.a.	4.27	−114.2	n.a.
$Mn_{0.50}Cd_{0.50}PS_3$[40]	4.25	4.18	−106	n.a.
$Mn_{0.20}Cd_{0.80}PS_3$[39]	n.a.	2.65	−39.7	n.a.
$NiPS_3$[41]	n.a.	n.a.	n.a.	58.0
$NiPS_3$[42]	2.94	n.a.	−241	60
$CoPS_3$[43]	4.90	3.87	−116	n.a.
$CoPS_3$[44]	4.90	n.a.	−223	n.a.

t.w. – this work, n.a. – not available, J/k_B exchange constant.[a] From susceptibility data.

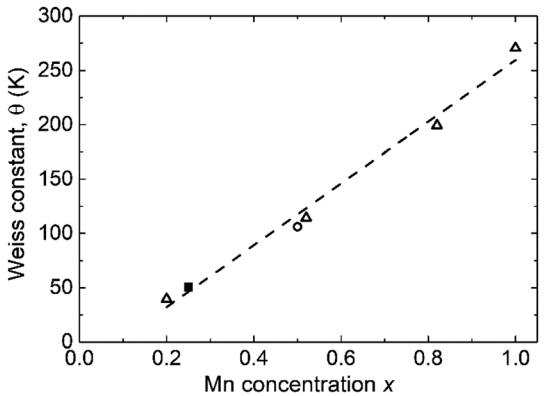

Fig. 4 The Weiss constant (θ) as a function of the Mn^{II} concentration in $Mn_xCd_{1-x}PS_3$. Triangles show data from,[39] circles data from,[40] while the square denotes the value obtained in the present study.

moments, $\mu_{eff} = 2.828(C)^{1/2}\ \mu_B$, for each compound. For the bimetallic phases, S is a linear average of the spin of the M^{II} ions.[40] The obtained values are shown in Table 3 and compared with previously reported data. The great difference between μ_{eff} and μ_{SO} (spin only value) found for $Co_{0.25}Cd_{0.75}PS_3$ suggests that the orbital momentum is not completely quenched.

The antiferromagnetic behaviour observed in the mentioned phases (Mn^{II}, Co^{II}, Ni^{II}) is an interesting result.

A possible explanation must be related to the sample preparation method. In the samples obtained by the ceramic process the 3d cations are distributed randomly,[28] while the intercalation and cationic exchange reaction should lead to an organized distribution of transition ions according to the vacancies, created by the first reaction.[29,30] Schmedt auf der Günne *et al.* proposed a model for the vacancies present in the $K_{0.5}Cd_{0.75}PS_3$ phase, which has been proved to be the same as in our materials.[35] According to this model and considering that the paramagnetic ions migrate into the same vacancies, the scheme shown in Fig. 5 can give a representation of the paramagnetic ion distribution after the cationic exchange reaction. It can be seen in this scheme, that the exchange interaction between paramagnetic ions must be established between third neighbours of the hexagonal arrangement. The inserted

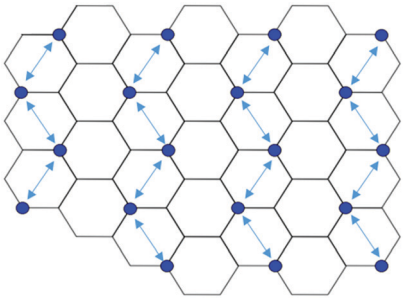

Fig. 5 Scheme of the distribution of the paramagnetic ions (blue dots).

magnetic 3d ions are bonded through a $P_2S_6^{4-}$ ligand on opposite sides of a hexagon (ligands are located at the centre of each hexagon). In this case, a lower percolation threshold is expected, in comparison with a random arrangement of ions. These ideas are corroborated by our NMR and SEM-EDXS results that lead to an occupation of 25% of the sites by magnetic ions. Long range order below the percolation threshold has already been discussed, highlighting the importance of interactions with second and third-nearest neighbours of the hexagonal arrangement for the determination of the percolation threshold.[6,21,22,45] Furthermore, it is known that the $MnPS_3$ phase has an ordered structure, where each paramagnetic ion is antiferromagnetically coupled with its three neighbours, while the $NiPS_3$ and $CoPS_3$ have a magnetic structure formed by ferromagnetic chains which are antiferromagnetically coupled.[5]

In all cases the interaction with the third neighbours is antiferromagnetic, consistent with our experimental results.[5]

The magnetization $M(H)$ curves were also analyzed. No peaks were observed in the $dM(H)/dH$ curves (Fig. S3, ESI‡) indicating that spin-flop phenomena are not present in the obtained materials. The absence of spin flop can be attributed to the nature and concentration of the cations. First of all, spin flop has been only observed in $MnPS_3$ phases.[3,46,47] Secondly, upon gradual replacing Mn^{II} by Mg^{II} ions the spin flop field decreases, becoming unobservable for Mn^{II} concentrations below 90%.[47]

EPR spectroscopy

The three bimetallic systems with paramagnetic cations were also analyzed by EPR spectroscopy.

The phase with Ni^{II} ions does not show an EPR spectrum even at low temperatures. It is known that if the environment of the centre is distorted, such that the magnitude of the zero-field splitting parameter D is higher than the conventional available microwave quantum, the Ni^{II} centres become EPR silent.[48]

In the case of phases with Co^{II} ions, EPR spectra can be recorded only at low temperatures and for $Co_{0.25}Cd_{0.75}PS_3$ they are observable only below 50 K (Fig. 6). Similar behaviour has been reported for other Co^{II} containing phases.[24] The spectrum is consistent with Co^{II} ions in a trigonally distorted octahedral environment,[24] due to the insertion of these cations in the vacancies of $K_{0.5}Cd_{0.75}PS_3$.

It is evident that hyperfine structure is not present in these spectra and to account for the physical mechanism we hypothesize that the Co^{II} ions are coupled among themselves by strong

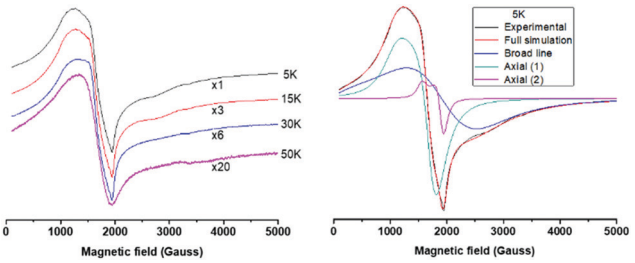

Fig. 6 EPR spectra of the $Co_{0.25}Cd_{0.75}PS_3$ phase at selected temperatures. Microwave frequency: 9.478 GHz. Left: Experimental results. Right: Simulation of the 5 K data.

exchange interactions. In the absence of exchange the hyperfine structure arising from a ^{59}Co nuclear spin (I = 7/2, abundance = 100%) would consist of eight equally spaced hyperfine lines having almost the same amplitude and width. When the hyperfine coupling constant A and the strength of the exchange interaction J are comparable, the exchange may produce broadening, narrowing, or a total collapse of the hyperfine structure into a single line, depending on the strength of the interactions.

It can be noted that the spectra of Fig. 6 (left) show broad features (at magnetic field strengths in the range 100–180 mT) and also sharp ones (at around 200 mT); this is typical of multicomponent spectra. It was thus impossible to simulate the spectra on the basis of a single set of Hamiltonian parameters. To give some insight into the problem we tried a multicomponent fitting of the 5 K spectrum, taking as parameters the g-tensor principal values and broadening effects caused by the homogeneous line width and magnetic field strain. The results are summarized in Fig. 6 (right) and Table 4 (see ESI‡ for further details). The fit comprises three components: the broadest one is based on an isotropic g-value and a homogeneous line width; the other two components have axial g-tensors. Since the result of the simulation fits the experimental data very closely, the simulation can be considered convincing. However, taking into account the nature of the analysis there is no guarantee that the above hypotheses are unique. Possibly, similarly convincing results might be obtained by other sets of components and parameters. We can hypothesize that the differences in g-values originate from different, structurally non-equivalent Co^{II} sites. Considering the magnetic nature of the Co^{II}–Co^{II} coupling we may further speculate that the apparent differences in g-values could reflect the effect of different local magnetic fields acting on the Co^{II} ions.

Table 4 Spin Hamiltonian and broadening parameters for the spectra of $Co_{0.25}Cd_{0.75}PS_3$ at 5 K

	Broad line	Axial (1)	Axial (2)
S	$\frac{1}{2}$	3/2	3/2
$g_\perp$	3.5534	3.9370	3.5459
$g_\parallel$	3.5534	6.0081	4.3552
lwpp(G)	39	0	5.9
lwpp(L)	111	29.9	10.0
HStrain$_\perp$	0	260	0
HStrain$_\parallel$	0	2008	0
Weight	200	4.82	0.36

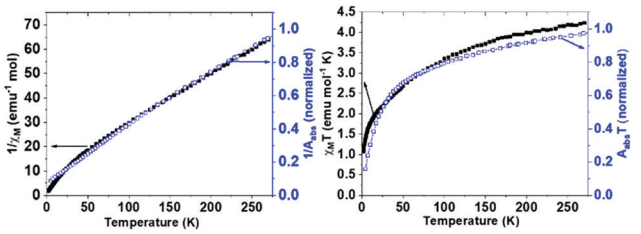

Fig. 7 Comparison of the data obtained from magnetic susceptibility (solid black squares) and EPR (open blue squares) for $Mn_{0.25}Cd_{0.75}PS_3$.

The spectra of the studied bimetallic phase with Mn^{II} ions (Fig. S4, ESI‡) show a single line in the whole temperature range. Apparently, the nuclear magnetic hyperfine splitting with ^{55}Mn is suppressed, due to strong interelectronic spin–spin interactions and/or exchange narrowing phenomena,[49] and therefore, a single line is observed.[11,50–53] Simulation and absolute intensities A_{abs}, as determined by the double integration of the obtained spectra, allow to compare these results with those of magnetic susceptibility (Fig. 7). From the curve of the temperature dependence of $1/A_{abs}$, a negative Weiss constant was obtained (θ = −47 K), which is found to be close to the one obtained from dc magnetic susceptibility (−50 K). Furthermore, the temperature dependence of $A_{abs} \times T$ also shows antiferromagnetic behaviour, decreasing in intensity at lower temperature. Therefore, for the $Mn_{0.25}Cd_{0.75}PS_3$ phase, the antiferromagnetic behaviour is confirmed by both techniques.

Electrical conductivity

In order to investigate the conductivity of these materials, they were analysed by broad band impedance spectroscopy. Fig. 8 presents the complex electrical conductivity (σ^*) of the different layered compounds as a function of frequency, where it is possible to observe that σ^* depends on the frequency. The presence of the different ions modifies the electrical conductivity with respect to that of the pristine $CdPS_3$ phase.

The electric modulus is defined as the inverse of dielectric permittivity, $M^* = 1/\varepsilon^*$, and the information that it provides is associated to microscopic electrical relaxations.[54,55] Fig. 9 presents the imaginary part (M''/M_{max}'') of the electric modulus of

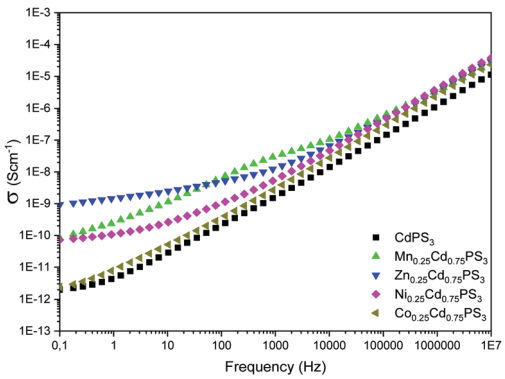

Fig. 8 Complex electrical conductivity as a function of frequency of bimetallic systems.

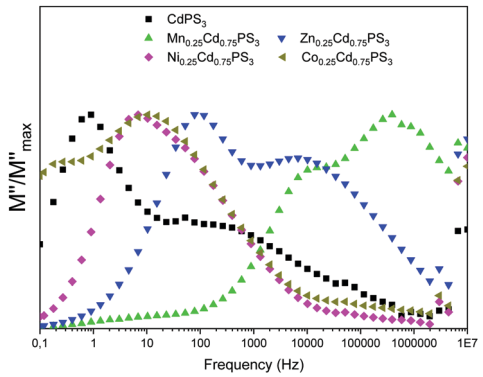

Fig. 9 Imaginary part of electric modulus as function of frequency of bimetallic systems.

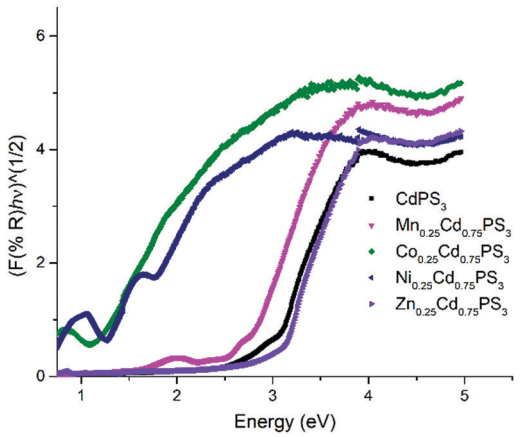

Fig. 10 Tauc plots for the studied lamellar phases.

$CdPS_3$ and that of the bimetallic systems. The data (which have been normalized by the corresponding M_{max}'' of each curve) show that the partial replacement of Cd^{II} affects the electrical relaxations of the bimetallic systems.

As the cations are inserted in the layers, these phases are not exactly intercalated systems, and the movement of the 3d-ions does not seem plausible. The occurrence of electronic hopping in mixed valence MPS_3 materials, which provides stability to the material has been reported.[43] However, due to the nature of the d-ions present, this phenomenon is unlikely in the studied bimetallic phases. It is important to mention that the complex electrical conductivity (σ^*) is increased in the bimetallic systems $Mn_{0.25}Cd_{0.75}PS_3$, $Zn_{0.25}Cd_{0.75}PS_3$ and $Ni_{0.25}Cd_{0.75}PS_3$ (Fig. 8). This may be attributed to the fact that the Mn^{II}, Zn^{II} and Ni^{II} ions induce the polarization of bonds in these bimetallic systems, as a consequence of the different electronegativity of the secondary ions compared to that of Cd^{II}, facilitating the charge transport. The charge motions of the induced polarized bonds are accompanied by electrical relaxation, as seen by the analysis of M''/M_{max}'' (Fig. 9). The highest value of conductivity is observed for $Zn_{0.25}Cd_{0.75}PS_3$ ($\sigma^* = 9.3 \times 10^{-10}$ S cm^{-1}), which is similar to that of semiconducting materials.[56]

This result suggests that a slight electronegativity difference between the metallic centres of a bimetallic system facilitates the charge motions, while higher electronegativity differences would hinder the charge motion. The only anomalous behaviour was observed for the Co^{II} phase, whose conductivity is close to that of the $CdPS_3$ phase. This phenomenon could be related to the fact that the Co^{II} and Cd^{II} phases are the only ones that present relaxation processes at lower frequencies, which could correspond to local relaxation processes. The latter may account for a lower charge mobility, and hence a lower electrical conductivity in these two materials.

Optical properties

These materials can also be classified as semiconductors by the value of the band gap energy. Fig. 10 shows the Tauc plots of the obtained bimetallic phases. The spectra of the three phases, with non-filled 3d shells, show at low energies weak bands due to d–d transitions. The obtained values for the energy gap are given in Table 5 (see Fig. S5 for the calculation of the values, ESI‡), together with some data from the literature.

Table 5 Band gap values for the studied mono and bimetalllic lamellar phases

Phase	GAP (eV)	Ref.
$CdPS_3$	2.95	This work
$Mn_{0.25}Cd_{0.75}PS_3$	2.68	This work
$Co_{0.25}Cd_{0.75}PS_3$	0.99	This work
$Ni_{0.25}Cd_{0.75}PS_3$	1.27	This work
$Zn_{0.25}Cd_{0.75}PS_3$	2.99	This work
$CdPS_3$	3.06	57
$NiPS_3$	1.59	58
	1.6	59
$ZnPS_3$	3.4	7
$CoPS_3$	1.4	60
$MnPS_3$	2.7	61
	2.5	62

From these data it is possible to conclude that the band gap energy is drastically modified by the insertion of Ni^{II} and Co^{II}. On the other hand, when Zn^{II} ions are inserted a band gap value close to that of the $CdPS_3$ phase is obtained. Table 5 indicates that this behavior correlates with the trend observed in the band gap values of the monometallic phases $M^{II}PS_3$ (M = Co, Ni, Mn, Zn), which are lower than that of $CdPS_3$ in the case of M = Co, Ni, Mn, and higher in the case of M = Zn. Thus the energy gaps of the bimetallic phases appear to be dominated by the monometallic system that has the lower band gap energy.

Conclusions

Four new ordered bimetallic phases of composition $M^{II}_{0.25}Cd_{0.75}PS_3$ (M = Ni, Co, Mn, Zn) were obtained by a two-step ion exchange reaction involving a freshly prepared $K_{0.5}Cd_{0.75}PS_3$ intermediate. The characterization by SEM-EDXS, solid state NMR, FTIR and powder X-ray diffraction confirms the migration of the inserted 3d ions from the interlayer space into the ordered vacancies of the layers of $K_{0.5}Cd_{0.75}PS_3$ precursor generating homogeneous materials. The properties of these materials were rationalized in relation to the distribution of the 3d ions within

the layers. Magnetic susceptibility data and EPR spectroscopy confirmed an antiferromagnetic coupling in the Mn^{II}, Ni^{II}, and Co^{II} substituted materials, which can be explained by the ordered distribution of the inserted 3d ions. The electrical conductivity of these bimetallic phases is dominated by the movements of small dipoles, created by the difference in electronegativity of the cations. The smaller the dipole, the higher is the conductivity. Finally, the band gap energies resemble the values of the pristine phase with the lower band gap values present in the bimetallic systems, probably due to an overlap of the band structures. Our results suggest that the physical properties of these materials are crucially linked to the ordered distribution of the 3d ions.

Conflicts of interest

There are no conflicts to declare.

Acknowledgements

PF acknowledges FONDECYT/CONICYT the postdoctoral grant 3170186. PF and ES thank Financiamiento Basal FB0807 (CEDENNA). PF, ES, NA are members of the LIA-M3 project 1207 (France/Chile). The authors thank CONICYT for the FONDEQUIP/PPMS/EQM 130086 grant for the purchase of a PPMS, which permitted the magnetic susceptibility measurements. Support by FAPESP, process numbers 2013/07793-6 (CEPID) and 2017/06649-0 (postdoctoral fellowship of CD), CNPq 427164/2018-4 and FAPEG 201410267001782 are gratefully acknowledged.

References

1 H. Hahn and W. Klingen, Über Sulfid- und Selenidphosphide des Eisens, Kobalts und Nickels, *Naturwissenschaften*, 1965, **52**, 494.

2 S. Y. Kim, T. Y. Kim, L. J. Sandilands, S. Sinn, M. C. Lee, J. Son, S. Lee, K. Y. Choi, W. Kim, B. G. Park, C. Jeon, H. Do Kim, C. H. Park, J. G. Park, S. J. Moon and T. W. Noh, Charge-Spin Correlation in van der Waals Antiferromagnet NiPS3, *Phys. Rev. Lett.*, 2018, **120**, 136402.

3 A. R. Wildes, V. Simonet, E. Ressouche, R. Ballou and G. J. McIntyre, The magnetic properties and structure of the quasi-two-dimensional antiferromagnet $CoPS_3$, *J. Phys.: Condens. Matter.*, 2017, **29**, 455801, DOI: 10.1088/1361-648X/aa8a43.

4 I. Cabria and A. A. El-Meligi, DFT simulation of hydrogen storage on manganese phosphorous trisulphide ($MnPS_3$), *Int. J. Hydrogen Energy*, 2018, **43**, 5903–5912.

5 F. Wang, T. A. Shifa, P. Yu, P. He, Y. Liu, F. Wang, Z. Wang, X. Zhan, X. Lou, F. Xia and J. He, New Frontiers on van der Waals Layered Metal Phosphorous Trichalcogenides, *Adv. Funct. Mater.*, 2018, **28**, 1–24.

6 M. A. Susner, M. Chyasnavichyus, M. A. McGuire, P. Ganesh and P. Maksymovych, Metal Thio- and Selenophosphates as Multifunctional van der Waals Layered Materials, *Adv. Mater.*, 2017, **29**, 1602852.

7 R. Brec, D. M. Schleich, G. Ouvrard, A. Louisy and J. Rouxel, Physical Properties of Lithium Intercalation Compounds of the Layered Transition Chalcogenophosphates, *Inorg. Chem.*, 1979, **18**, 1814–1818.

8 N. Ismail, M. Madian and A. A. El-Meligi, Synthesis of $NiPS_3$ and CoPS and its hydrogen storage capacity, *J. Alloys Compd.*, 2014, **588**, 573–577.

9 L. Silipigni, A. Basile, F. Barreca, G. De Luca, L. Monsù Scolaro, B. Fazio and G. Salvato, Partial reduction of graphene oxide upon intercalation into exfoliated manganese thiophosphate, *Philos. Mag.*, 2017, **97**, 2484–2495.

10 R. Clement, A novel route to intercalation into layered $MnPS_3$, *J. Chem. Soc., Chem. Commun.*, 1980, 647.

11 P. Fuentealba, V. Paredes-Garcia, D. Venegas-Yazigi, I. D. A. Silva, C. J. Magon, R. Costa de Santana, N. Audebrand, J. Manzur and E. Spodine, Magnetic properties of composites based on the intercalation of Zn^{II} and Cu^{II} bimetallic macrocyclic complexes in the $MnPS_3$ phase, *RSC Adv.*, 2017, **7**, 33305–33313.

12 E. Spodine, P. Valencia-Gálvez, P. Fuentealba, J. Manzur, D. Ruiz, D. Venegas-Yazigi, V. Paredes-García, R. Cardoso-Gil, W. Schnelle and R. Kniep, Magnetic behavior of $MnPS_3$ phases intercalated by $[Zn_2L]^{2+}$ (LH_2: macrocyclic ligand obtained by condensation of 2-hydroxy-5-methyl-1,3-benzenedicarbaldehyde and 1,2-diaminobenzene), *J. Solid State Chem.*, 2011, **184**, 1129–1134.

13 X. Zhang, H. Zhou, X. Su, X. Chen, C. Yang, J. Qin and M. Inokuchi, Synthesis, characterization and magnetic properties of transition metal salen complexes intercalated into layered $MnPS_3$, *J. Alloys Compd.*, 2007, **432**, 247–252.

14 M. Evain, F. Boucher, R. Brec and Y. Mathey, The question of silver pairing in the new structurally resolved two-dimensional phase $Ag_2MnP_2S_6$, *J. Solid State Chem.*, 1991, **90**, 8–16.

15 Y. Mathey, R. Clement, C. Sourisseau and G. Lucazeau, Vibrational study of layered MPX_3 compounds and of some intercalates with $Co(.eta.5\text{-}C_5H_5)^{2+}$ or $Cr(.eta.6\text{-}C_6H_6)^{2+}$, *Inorg. Chem.*, 1980, **19**, 2773–2779.

16 W. L. Hemme, W. Fujita, K. Awaga and H. Eckert, Intercalation of stable organic radicals into layered inorganic host matrices: Preparation and structural characterization of $Cd_{1-x}PS_3(metaMPYNN)2_x$, *J. Solid State Chem.*, 2009, **182**, 3330–3341.

17 D. Yang and R. F. Frindt, Structure of polymer intercalated $MnPS_3$ and $CdPS_3$, *J. Mater. Res.*, 2000, **15**, 2408–2413.

18 C. O. Oriakhi and M. M. Lerner, Rapid and Quantitative Displacement of Poly(ethylene oxide) from $MnPS_3$ and Other Layered Hosts, *Chem. Mater.*, 1996, **8**, 2016–2022.

19 J. S. O. Evans, D. O'Hare, R. Clement, A. Leaustic and P. Thuéry, Origins of the spontaneous magnetization in $MnPS_3$ Intercalates: A Magnetic Susceptibility and Powder Neutron Diffraction Study, *Adv. Mater.*, 1995, **7**, 735–739.

20 J. S. O. Evans, D. O'Hare and R. Clement, The Structure of $Co(.eta.\text{-}C_5H_5)^{2+}$ and NMe^{4+} Intercalates of $MnPS_3$: An X-ray,

Neutron-Diffraction, and Solid-State NMR Study, *J. Am. Chem. Soc.*, 1995, **117**, 4595–4606.
21 D. J. Goossens and T. J. Hicks, The magnetic phase diagram of $Mn_xZn_{1-x}PS_3$, *J. Phys.: Condens. Matter*, 1998, **10**, 7643–7652.
22 A. M. Mulders, J. C. P. Klaasse, D. J. Goossens, J. Chadwick and T. J. Hicks, High-field magnetization in the diluted quasi-two-dimensional Heisenberg antiferromagnet $Mn_{1-x}Zn_xPS_3$, *J. Phys.: Condens. Matter*, 2002, **14**, 8697–8705.
23 W.-C. Zheng and S.-Y. Wu, Explanation of the EPR g factors for Co^{2+} impurities in trigonal $Cd_2P_2S_6$ crystal, *Phys. Rev. B: Condens. Matter Mater. Phys.*, 2001, **307**, 28–33.
24 M. A. Hefni, N. Nagasundaram, D. Kreszowski and A. H. Francis, ESR studies of inter- and intra-lamellar cation exchange processes in $Cd_2P_2S_6$, *J. Phys. Chem. Solids*, 1990, **51**, 1405–1411.
25 D. Ruiz-León, V. Manríquez, J. Kasaneva and R. E. Avila, Insertion of trivalent cations in the layered MPS_3 (Mn, Cd) materials, *Mater. Res. Bull.*, 2002, **37**, 981–989.
26 E. Y. Goh, E. J. Kim and S. J. Kim, Structure modification on quaternary rare earth thiophosphates: $NaYbP_2S_6$, $NaSmP_2S_6$, and $KSmP_2S_7$, *J. Solid State Chem.*, 2001, **160**, 195–204.
27 Y. Wu and W. Bensch, Structural diversity of rare earth and transition metal thiophosphates, *CrystEngComm*, 2010, **12**, 1003–1015.
28 D. J. Goossens, A. J. Studer, S. J. Kennedy and T. J. Hicks, The impact of magnetic dilution on magnetic order in $MnPS_3$, *J. Phys.: Condens. Matter*, 2000, **12**, 4233–4242.
29 P. Fuentealba, C. Cortés, N. Audebrand, E. Le Fur, V. Paredes-García, D. Venegas-Yazigi, J. Manzur and E. Spodine, First copper(II) phase $M'_{0.2}Mn_{0.8}PS_3{\cdot}0.25H_2O$ and analogous M′ = Co^{II}, Ni^{II} and Zn^{II} materials obtained by microwave assisted synthesis, *Dalton Trans.*, 2015, **44**, 12493–12496.
30 P. Fuentealba, C. Cortes, J. Manzur, V. Paredes-García, D. Venegas-Yazigi, I. D. A. Silva, R. C. De Santana, C. J. Magon and E. Spodine, Magnetic behaviour of bimetallic layered phases $M'_{0.2}Mn_{0.8}PS_3{\cdot}0.25H_2O$ (M′ = Zn^{II}, Cu^{II}, Ni^{II}, Co^{II}), *Dalton Trans.*, 2017, **46**, 14373–14381.
31 J. Rodríquez-Carvajal and T. Roisnel, Line Broadening Analysis Using FullProf: Determination of Microstructural Properties, *Mater. Sci. Forum*, 2004, **443–444**, 123–126.
32 T. Roisnel and J. Rodríquez-Carvajal, WinPLOTR: A Windows Tool for Powder Diffraction Pattern Analysis, *Mater. Sci. Forum*, 2001, **378–381**, 118–123.
33 G. Ouvrard, R. Brec and J. Rouxel, Structural determination of some MPS_3 layered phases (M = Mn, Fe, Co, Ni and Cd), *Mater. Res. Bull.*, 1985, **20**, 1181–1189.
34 D. Louër and A. Boultif, Some further considerations in powder diffraction pattern indexing with the dichotomy method, *Powder Diffr.*, 2014, **29**, S7–S12.
35 J. Schmedt auf der Günne, H. Eckert, A. Léaustic and F. Babonneau, Vacancy ordering and host–guest interactions in $CdPS_3$ intercalates: Results from multidimensional solid state NMR, *Phys. Chem. Chem. Phys.*, 2003, **5**, 1306.
36 J. K. Furdyna, Diluted magnetic semiconductors, *J. Appl. Phys.*, 1988, **64**, R29–R64.
37 N. Chandrasekharan and S. Vasudevan, Dilution of a layered antiferromagnet: Magnetism in $Mn_xZn_{1-x}PS_3$, *Phys. Rev. B: Condens. Matter Mater. Phys.*, 1996, **54**, 14903–14906.
38 P. Fuentealba, V. Paredes-Garcia, D. Venegas-Yazigi, I. D. A. Silva, C. J. Magon, R. Costa de Santana, N. Audebrand, J. Manzur and E. Spodine, Magnetic properties of composites based on the intercalation of Zn^{II} and Cu^{II} bimetallic macrocyclic complexes in the $MnPS_3$ phase, *RSC Adv.*, 2017, **7**, 33305–33313.
39 X. Zhang, X. Su, X. Chen, J. Qin and M. Inokuchi, The synthesis and magnetism of mixed metal hexathiohypodiphosphate ($Mn_xCd_{1-x}PS_3$) system and its intercalates, *Microporous Mesoporous Mater.*, 2008, **108**, 95–102.
40 V. Manríquez, P. Barahona and O. Peña, Physical properties of the cation-mixed M′MPS_3 phases, *Mater. Res. Bull.*, 2000, **35**, 1889–1895.
41 N. Chandrasekharan and S. Vasudevan, Magnetism and exchange in the layered antiferromagnet $NiPS_3$, *J. Phys.: Condens. Matter*, 1994, **6**, 4569–4579.
42 P. a. Joy and S. Vasudevan, Magnetism in the layered transition-metal thiophosphates MPS_3 (M = Mn, Fe, and Ni), *Phys. Rev. B: Condens. Matter Mater. Phys.*, 1992, **46**, 5425–5433.
43 R. Brec, Review on structural and chemical properties of transition metal phosphorous trisulfides MPS_3, *Solid State Ionics*, 1986, **22**, 3–30.
44 C. C. Mayorga-Martinez, Z. Sofer, D. Sedmidubský, Š. Huber, A. Y. S. Eng and M. Pumera, Layered Metal Thiophosphite Materials: Magnetic, Electrochemical, and Electronic Properties, *ACS Appl. Mater. Interfaces*, 2017, **9**, 12563–12573.
45 D. J. Goossens, A. J. Studer, S. J. Kennedy and T. J. Hicks, The impact of magnetic dilution on magnetic order in $MnPS_3$, *J. Phys.: Condens. Matter*, 2000, **12**, 4233–4242.
46 A. R. Wildes, V. Simonet, E. Ressouche, G. J. McIntyre, M. Avdeev, E. Suard, S. A. J. Kimber, D. Lançon, G. Pepe, B. Moubaraki and T. J. Hicks, Magnetic structure of the quasi-two-dimensional antiferromagnet $NiPS_3$, *Phys. Rev. B: Condens. Matter Mater. Phys.*, 2015, **92**, 1–11.
47 D. J. Goossens and T. J. Hicks, Investigation of the temperature/field/composition magnetic phase diagram of $Mn_{1-x}Mg_xPS_3$, *J. Magn. Magn. Mater.*, 1998, **177–181**, 721–722.
48 J. Krzystek, J. H. Park, M. W. Meisel, M. A. Hitchma, H. Stratemeier, L. C. Brunel and J. Telser, EPR spectra from 'EPR-Silent' species: High-frequency and high-field EPR spectroscopy of pseudotetrahedral complexes of Nickel(II), *Inorg. Chem.*, 2002, **41**, 4478–4487.
49 P. W. Anderson and P. R. Weiss, Exchange Narrowing in Paramagnetic Resonance, *Rev. Mod. Phys.*, 1953, **25**, 269–276.
50 P. a. Joy and S. Vasudevan, Magnetism and spin dynamics in $MnPS_3$ and pyridine intercalated $MnPS_3$: An electron paramagnetic resonance study, *J. Chem. Phys.*, 1993, **99**, 4411–4422.
51 M. K. Bhide, M. D. Sastry, J. Qin, C. Yang, K. Yakushi, Y. Nakazawa, K. Ichimura, A. K. Sra and J. V. Yakhmi, Electron magnetic resonance studies of the intercalation ferromagnet 2,2′-bipyridine-$MnPS_3$ above and below Curie

temperature, *C. R. Seances Acad. Sci., Ser. C*, 2001, **4**, 189–192.

52 Y. Köseoglu, F. Yildiz, J. V. Yakhmi, J. Qin, X. Chen and B. Aktaş, EPR studies on BEDT-TTF intercalated $MnPS_3$ molecular magnet, *J. Magn. Magn. Mater.*, 2003, **258–259**, 416–418.

53 Y. Köseoğlu, R. Yilgin, J. V. Yakhmi, J. Qin, X. Chen and B. Aktas, X-,K- and Q-band ESR studies on intercalated $Fe_{0.9}PS_3(Phen)_{0.4}$, *J. Magn. Magn. Mater.*, 2003, **258–259**, 141–143.

54 K. L. Ngai and C. León, Relating macroscopic electrical relaxation to microscopic movements of the ions in ionically conducting materials by theory and experiment, *Phys. Rev. B: Condens. Matter Mater. Phys.*, 1999, **60**, 9396–9405.

55 P. B. Macedo, C. T. Moynihan and R. Bose, The Role of Ionic Diffusion in Polarization in Vitreous Ionic Conductors, *Phys. Chem. Glasses*, 1972, **13**, 171–179.

56 D. Chattopadhyay and P. C. Rakshit, *Electronics: Fundamentals and Applications*, New Age International Publishers, 8th edn, 2007.

57 C. Calareso, V. Grasso and L. Silipigni, Optical spectra of the layered $Cd_2P_2S_6$ and $Cd_2P_2Se_6$ compounds in the region from 1.6 to 5.5 eV, *J. Appl. Phys.*, 1997, **82**, 6228–6234.

58 P. J. S. Foot, J. Suradi and P. A. Lee, Optical and electronic properties of the layered semiconductors $NiPS_3$ and $FePS_3$, *Mater. Res. Bull.*, 1980, **15**, 189–193.

59 N. Kurita and K. Nakao, Band Structure of Magnetic Layered Semiconductor $NiPS_3$, *J. Phys. Soc. Jpn.*, 1989, **58**, 232–243.

60 R. Brec, G. Ouvrard, A. Louisy, J. Rouxel and A. Le Mehaute, The influence, on lithium electrochemical intercalation, of bond ionicity in layered chalcogenophosphates of transition metals, *Solid State Ionics*, 1982, **6**, 185–190.

61 P. Jeevanandam and S. Vasudevan, Magnetism in $MnPSe_3$: a layered 3d5 antiferromagnet with unusually large XY anisotropy, *J. Phys.: Condens. Matter*, 1999, **11**, 3563–3570.

62 P. Fuentealba, C. Cortés, N. Audebrand, E. Le Fur, V. Paredes-García, D. Venegas-Yazigi, J. Manzur and E. Spodine, First copper(II) phase $M'_{0.2}Mn_{0.8}PS_3{\cdot}0.25H_2O$ and analogous M′ = Co^{II}, Ni^{II} and Zn^{II} materials obtained by microwave assisted synthesis, *Dalton Trans.*, 2015, **44**, 12493–12496.

